

Imprints of M87 Jet Precession on the Black Hole-Accretion Disk System

Yuzhu Cui^{1,2*} and Weikang Lin^{2*}

^{1*}Research Center for Astronomical Computing, Zhejiang Lab, Hangzhou 311100, China.

^{2*}South-Western Institute For Astronomy Research, Yunnan University, Kunming 650500, Yunnan, P. R. China.

*Corresponding author(s). E-mail(s): yuzhu.cui@zhejianglab.com; weikanglin@ynu.edu.cn;

Abstract

Observational constraints on the configuration of the black hole (BH)-accretion disk-jet system are crucial for addressing key questions in black hole growth, accretion disk physics, and jet formation. The recently reported jet precession in M87 provides a novel avenue to explore these long-standing issues. This precession, attributed to the accretion disk's response to the frame-dragging effect of a spinning supermassive black hole (SMBH), indicates a non-zero spin. The relatively short precession period (~ 11 years) implies a compact accretion disk. In contrast to the traditional view of a strictly collimated shape, the M87 jet is inferred to curve at the innermost regions connecting to the spinning BH, which explains the unexpectedly wide innermost projected jet width.

1 Introduction

The nearby radio galaxy M87 is the first observational record of an astrophysical jet reported in 1918 [1]. Despite extensive studies, several fundamental aspects of its central engine remain uncertain. While the SMBH at the core of M87 is accreting at a low rate through a geometrically thick, radiatively inefficient accretion flow [2–5], the exact structure, size, and orientation of the accretion disk are poorly constrained by current observations. Additionally, determining the SMBH spin in M87 has proven challenging. Traditional

techniques like X-ray reflection spectroscopy [6, 7] and thermal continuum fitting [8, 9] are limited by the thick geometry and low accretion rate of the disk, making them unsuitable for M87. Although the Event Horizon Telescope (EHT) imaged the shadow of M87’s SMBH at 230 GHz, yielding robust estimates of its mass [10], stringent constraints on the black hole’s spin have remained elusive. As relativistic jets in active galactic nuclei (AGNs) are fundamentally linked to the SMBH and the surrounding accretion disk [11, 12], observations that probe the innermost regions of the BH-disk-jet system are essential for addressing these longstanding questions. M87—a powerful AGN hosting a SMBH and an extended relativistic jet—provides an ideal laboratory for such investigations [13–22].

Recent high-resolution observations of the M87 jet at milliarcsecond (mas) and sub-mas scales have provided crucial new insights into the above challenges [23, 24]. Notably, Cui et al. (2023) identified a periodic variation in the jet position angle, with a cycle of approximately 11 years, interpreted as Lense-Thirring (LT) precession due to a tilted accretion disk [24]. LT precession, a relativistic effect caused by frame-dragging near the SMBH [25], offers a unique opportunity to infer properties of the black hole-disk system that are otherwise difficult to measure directly. In this work, we demonstrate that the observed jet precession provides stringent constraints on the SMBH spin and accretion disk parameters. In addition, the precession implies that the jet is not perfectly collimated, particularly in its innermost regions, addressing the projected jet width discrepancy reported by [23]. The combination of the jet’s precession and its inner width profile reveals a coherent picture of the global jet structure, tightly linked to the properties of the SMBH.

2 The SMBH spin and accretion disk size

Due to computational cost and technical issues, comprehensive numerical studies of tilted and geometrically thick accretion disks were not possible until recently [26, 27]. In particular, the main body of the disk undergoes LT precession [26, 27], and the jet follows the disk and precesses with the same period [24, 28, 29]. The precession period can be calculated by

$$T_{\text{prec}} \simeq \frac{\pi c^2 r_{\text{LT}}^3}{G a M^2} \frac{1 + a \left(\frac{r_{\text{g}}}{r_{\text{LT}}}\right)^{3/2}}{1 - \frac{3}{4} a \left(\frac{r_{\text{g}}}{r_{\text{LT}}}\right)^{1/2}}, \quad (1)$$

where we have taken into account the sense of the accretion flow orbit concerning the central SMBH spin and some higher-order corrections [30]. In the above, $a \equiv Jc/GM^2 \in [-1, 1]$ is the dimensionless spin parameter and a positive (negative) a corresponds to a prograde (retrograde) disk, M is the SMBH mass, and $r_{\text{g}} = GM/c^2$ is the gravitational radius, J the spin angular momentum, G is the gravitational constant, and c is the speed of light. Note that r_{LT} is the effective radius that depends on the mass distribution of the part of the disk that exhibits a coherent precession. For M87, the reported precession period

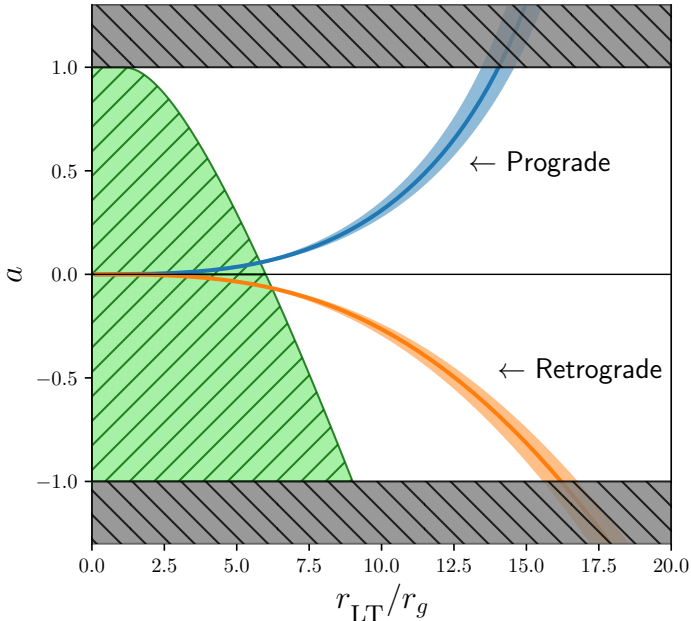


Fig. 1 The constraint on M87 BH spin parameter-effective disk LT radius relation from the observed jet precession period and SMBH mass. The gray-shaded region is not allowed since the BH spin $a \in [-1, 1]$ physically. The green shaded region is not allowed since we conservatively require $r_{\text{LT}} > r_{\text{ISCO}}$ when the disk rotation is prograde with respect to the SMBH spin. The blue (orange) curve corresponds to a prograde (retrograde) disk.

$T_{\text{prec}} = 11.24 \pm 0.47$ years [24] and the SMBH mass $M_{\text{M87}} = (6.5 \pm 0.7) \times 10^9 M_{\odot}$ (where M_{\odot} is the solar mass) [10] put a constraint on the a - r_{LT} space which is shown in Fig. 1.

For the same $|a|$, the required r_{LT} is somewhat smaller for a prograde disk compared to a retrograde disk. The relatively short precession period puts a tight constraint on the disk size and requires $r_{\text{LT}} \leq 14.0_{-0.6}^{+0.5} r_g$ for the prograde case and $r_{\text{LT}} \leq 16.2 \pm 0.6 r_g$ for the retrograde case. The equal sign corresponds to the case of maximum rotation, i.e. $a = 1$ or $a = -1$. Thus, the accretion disk is constrained to be rather compact in the sense that the effective LT radius is at most around $15 r_g$.

The constraint on a is highly sensitive to r_{LT} . Assuming $r_{\text{LT}} > r_{\text{ISCO}}$ where r_{ISCO} is the innermost stable circular orbit [31], we establish a lower limit of $a \gtrsim 0.06$ [24]. Although it provides a weak constraint on the value of a , the non-spinning scenario is successfully excluded. However, considering the extended size of the accretion disk, the assumption $r_{\text{LT}} > r_{\text{ISCO}}$ is highly conservative. Analyzing the structure of the disk provides a deeper understanding into the properties of the system. To achieve this, we follow [27, 32] and adopt a power-law surface density profile with $\sigma(r) \propto r^{-\zeta}$ for the co-precessing part of the disk. A positive (negative) ζ represents a disk that is more concentrative inwards (outwards), and $\zeta = 0$ represents a constant surface density. The

co-precessing disk is truncated, with r_{in} (r_{o}) denoting the inner (outer) edge of it. It is important to emphasize that the outer radius here refers to that of the co-precessing bulk of the accretion disk, which may not be the edge of the whole disk, whose definition is not clear. With these settings, the effective LT radius then reads [27],

$$r_{\text{LT}} = r_{\text{o}} \left(\frac{1 + 2\zeta (r_{\text{in}}/r_{\text{o}})^{1/2+\zeta} [1 - (r_{\text{in}}/r_{\text{o}})^{5/2-\zeta}]}{5 - 2\zeta} \frac{1 - (r_{\text{in}}/r_{\text{o}})^{5/2-\zeta}}{1 - (r_{\text{in}}/r_{\text{o}})^{1/2+\zeta}} \right)^{1/3}. \quad (2)$$

It is justified to assume $r_{\text{in}} > r_{\text{ISCO}}$, which sets a lower limit of a for a given r_{o} and profile index ζ . On the other hand, $r_{\text{in}} < r_{\text{o}}$ is geometrically required, which sets an upper limit of a for a given r_{o} . Taking $T_{\text{prec}} = 11.24$ years [24] and $M_{\text{M87}} = 6.5 \times 10^9 M_{\odot}$ [10], the resultant constraint on the a - r_{o} space, capturing $r_{\text{ISCO}} < r_{\text{in}} < r_{\text{o}}$, are shown by the shaded areas in Fig. 2. These constraints are presented for three selected values of ζ , with different senses of the disk orbit considered separately.

The General relativistic magnetohydrodynamic (GRMHD) simulations indicate that the disk surface density is nearly constant ($\zeta = 0$) [27], which we denote as the fiducial case. For this scenario, the outer radius of the disk is maximally $\sim 42 r_{\text{g}}$ ($25 r_{\text{g}}$) for a prograde (retrograde) disk, further suggesting a rather compact disk. The size of the disk is sensitive to the profile index ζ . In general, a larger ζ allows a larger outer radius because a mass profile more concentrated inwards permits a larger r_{o} to achieve the same r_{LT} . For a fairly inward-concentrated and prograde disk with $\zeta = 1$, the outer radius can be up to $\sim 194 r_{\text{g}}$ for a maximally spinning SMBH.

For aligned accretion disks, prograde cases generally lead to a larger disk compared to retrograded cases because r_{ISCO} is smaller, allowing r_{in} to be smaller. For tilted accretion disks, this may not be true. Simulations show that the inner radius of a disk with a modest tilt for a prograde case is nearly independent of the spin [33]. This suggests that even for a highly spinning black hole, the inner radius of the disk might not shrink with r_{ISCO} , and the tight constraint on the outer radius might not be relaxed. We illustrate the cases with $r_{\text{in}} = 6 r_{\text{g}}$ by the red curves in the upper panels of Fig. 2. Even though retrograde disk cases have not been studied in simulations, it is reasonable to assume that $r_{\text{in}} > r_{\text{ISCO}}$ still holds. Therefore, the conclusion that r_{in} is nearly constant might not apply to retrograde disks.

The high-resolution observations of the emission surrounding the black hole, as directly resolved by the ongoing long-term monitoring efforts with the EHT, is crucial to more accurately determine the SMBH spin. Combined with the constraints from jet precession presented here, this will significantly refine our understanding of disk properties, such as outer radius and profile index, which are influenced by intrinsic factors including temperature, density, and viscosity.

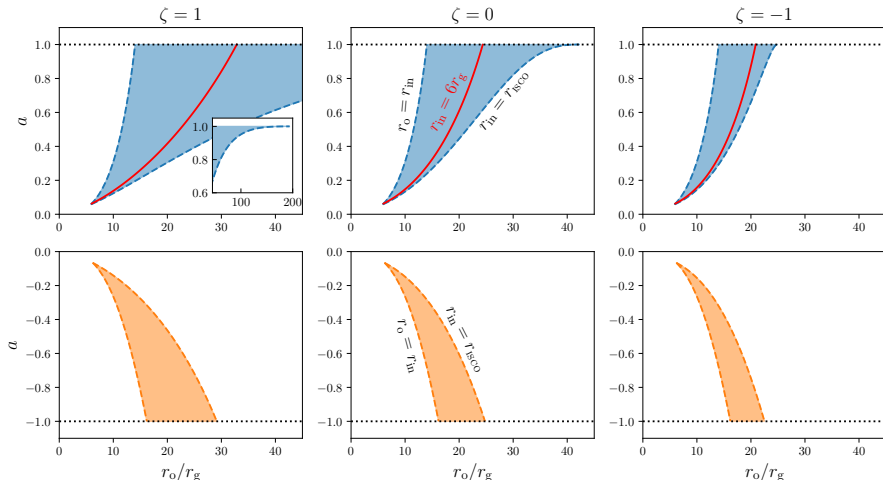


Fig. 2 Constraints on the M87 BH spin and accretion disk morphology in the a - r_o (disk outer radius) parameter space. The upper (lower) panels are for prograde (retrograde) disks. A larger profile index ζ represents a disk that is more concentrated inwards. The shaded areas enclose the allowed region where $r_{\text{ISCO}} < r_{\text{in}} < r_o$. The red curves represent the cases where $r_{\text{in}} = 6 r_g$ motivated by the finding in simulations that the inner radius for prograde tilted disks is insensitive to the black hole spin [33].

3 The jet structure and the innermost jet width

The second important implication concerns the jet’s structure. The observed precession of the M87 jet challenges the traditional view of it being strictly collimated. Instead, the jet precesses around the central SMBH’s spin axis. On the one hand, the inferred precession angle should be understood as the angle between the SMBH spin and the tangential direction of the jet axis at the corresponding scale. The small precession angle observed at the mas scales indicates that the SMBH spin is nearly aligned with the large-scale jet. Based on this information, it can be inferred that the spin vector of the M87 SMBH is oriented away from the Earth, assuming a finite spin value [4]. On the other hand, observations have confirmed that the jet becomes well-collimated at larger scales [20, 34, 35]. These suggest that the jet is not a rigid structure, and the tangential angle with respect to the SMBH spin (referred to as the precession angle) decreases with distance from the central SMBH. We parameterize the precession angle ψ as a function of the jet intrinsic length ρ by

$$\psi(\rho) = \psi_{\text{in}} \times \left(0.5 - \frac{1}{\pi} \arctan\left(\frac{\log_{10} \rho - \log_{10} \rho_t}{\Delta}\right) \right), \quad (3)$$

where ψ_{in} is the precession angle at the innermost region of the jet, ρ_t denotes the transition location, and Δ represents the transition width. The right panel of Fig. 3 illustrates the 3D structure of the resultant jet.

Observations of the jet structure and dynamics at various scales, especially at sub-mas scales, are crucial for fully understanding the detailed structure

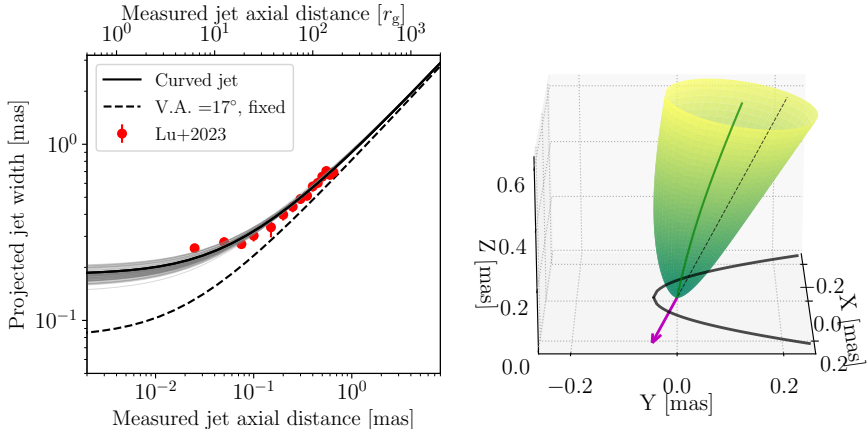


Fig. 3 Curved jet at the innermost region. *Left:* The red points are projected jet width profile adopted from Lu et al. (2023) [23] which were measured from the observation with GMVA + ALMA + GLT at 86 GHz in 2018. The dotted curve shows the projected jet width of the collimated jet with $a = 0.9$ viewed from a fixed viewing angle $\phi = 17^\circ$ [23, 35, 36] while the solid curve indicates the corresponding projected jet width of a curved jet with the best-fit parameters. The light curves are prediction with randomly selected samples obtained from an MCMC analysis and represent the uncertainty of the fitting. The precession angle at mas scales, $(1.25 \pm 0.18)^\circ$ [24], was incorporated into the MCMC analysis. *Right:* 3D configuration of jet structure and the corresponding projected profile on the sky plane. Z -axis is set along with LOS. The positive z represents the direction pointing towards the Earth and the X - Y panel indicates the sky panel. The green cone is the jet and the green line is the jet axis. The magenta arrow denotes the BH spin, which is aligned with the black dashed line representing the precession axis.

of the jet. In this context, the current jet precession observed at $0.7 \sim 3$ mas [24] and the innermost jet structure [23] provide significant constraints. In particular, Lu et al. (2023) reported an unexpectedly large jet width at $\lesssim 0.1$ mas [23], which can be explained by a smaller viewing angle at those scales. A smaller viewing angle can naturally occur in a precessing jet model where the jet is in a phase nearly coplanar with the line of sight (LOS) and the precession axis. The position angle of the jet at $\lesssim 0.1$ mas aligns roughly with that at larger scales, further suggesting that the inner jet precession is in such a phase. For simplicity, we assume that the inner jet is exactly coplanar with the LOS and the precession axis at the time of the observation (2018).

To demonstrate that the curved jet model, inspired by the observed jet precession, effectively addresses the reported anomaly in the innermost jet width, we analyze the projected jet width profile and compare it with the measurements from Lu et al. (2023). The shape of an uncurved jet is modeled by a nearly parabolic cone along the Z -axis,

$$W = \frac{C}{2} \rho^\alpha, \quad (4)$$

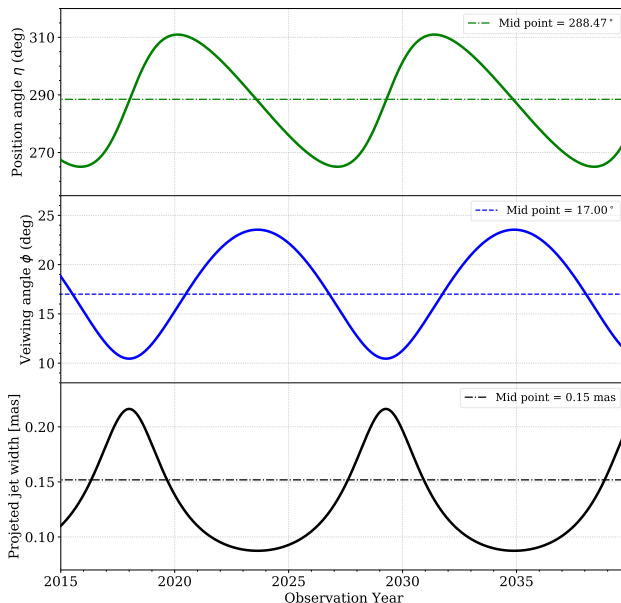


Fig. 4 Prediction of the evolution of the projected position angle η , the viewing angle ϕ and the projected jet width by the curved jet model with the best-fit parameters at the core separation $r = 0.02$ mas.

where W represents the intrinsic jet width. The parameters $C = 0.19$ and $\alpha = 0.6$ are determined by matching the predicted profile of projected jet width for the uncurved jet case with $a = 0.9$ [23, 35, 36]. The jet is then curved according to the parameterized precession angle (Eq. (3)) and projected onto the plane perpendicular to the LOS to derive the predicted jet width as a function of the measured jet axial distance (see Appendix A for details). To account for the precession observation by Cui et al. (2023) [24], a prior on the precession angle of $(1.25 \pm 0.18)^\circ$ at 1.8 mas is incorporated into the analysis. In the left panel of Fig. 3, we compare the predicted jet width profile with observations from Lu et al. (2023) [23]. The curved jet model predicts a wider jet width (solid curve) than the collimated jet model (dashed curve) at distances $\lesssim 0.1$ mas, while maintaining similar jet widths at larger scales. The prediction of the best-fit precessing curved jet model with $\psi_{\text{in}} = 11.1^\circ$, $\rho_t = 100 r_g$ and $\Delta = 0.40$ aligns closely with the observed data (red dots).

Continuous monitoring of the innermost jet is crucial to test the above hypothesis. As the jet precesses, both its position angle and viewing angle vary, especially at the innermost scales. The top and middle panels of Fig. 4 illustrate the time evolution of these angles on a scale of 0.02 mas. Importantly, the larger precession angle in the innermost region causes the viewing angle to decrease when the jet approaches LOS. This results in an asymmetrical time variation curve for the position angle, which exhibits a skewness. The direction of this skewness is determined by the sense of precession and, therefore, by

the direction of the SMBH spin, offering a potential test of the SMBH’s spin direction that is inferred to point away from Earth as mentioned above. While the time variation of the viewing angle is more challenging to observe directly, it leads to changes in the jet width, as shown in the bottom panel of Fig. 4. Long-term observations resolving sub-mas scales [16, 18, 23] are promising for detecting variations in both the position angle and jet width in this region.

A Curved jet and the innermost jet projected width

As demonstrated in Section 3, the innermost jet may have a larger precession angle, which can explain the unexpectedly large measured jet width at $\lesssim 0.1$ mas reported in Lu et al. (2023) [23]. Here, we highlight the technical details about the curved jet modeling and parameter inference. We assume that the edge shape of the 3D jet can be parameterized by a nearly parabolic function given in Eq. (4). Both W and ρ there are measured in mas, with a conversion factor of $1 \text{ mas} = 250 r_g$ for M87.

We begin by reproducing the theoretical prediction of the jet width as a function of the measured axial distance for $a = 0.9$. The coordinate system is defined with the X - Y plane perpendicular to LOS and the Z axis pointing towards the observer. We construct a parabolic cone along the Z direction, which is then tilted by 17° in the Z - Y plane. The projection of this cone onto the X - Y plane represents the 2D jet observed. The right panel of Fig. 3 illustrates the schematic of a tilted jet and its projection on the X - Y plane (the depicted case of a curved jet will be discussed later). In this projection, the width in the X -direction corresponds to the observed jet width, and the Y -coordinate corresponds to the observed axial distance. By matching the predicted jet width as a function of the axial distance, we determine the parameters $C = 0.19$ and $\alpha = 0.6$. In Fig. 5, the left panel presents a 3D view of the curved jet from an edge-on view. The middle panel illustrates the 2D structure of the jet axis, while the right panel displays the profiles of the precession angle and the viewing angle.

The scenario described above is the standard case assumed in the analysis of Lu et al. (2023) [23]. In contrast, our curved jet model proposes that, rather than forming a collimated cone, the angle between the jet and its precession axis (referred to as the precession angle, ψ) decreases from a finite value near the core to zero at large distances as parameterized by Eq. (3). Motivated by the observation that the angle of position of the jet at scales $\lesssim 0.1$ mas is similar to that at larger scales, the precession of the innermost jet is likely in a phase in which the innermost jet, the large-scale jet and the LOS are nearly coplanar. Consequently, the jet viewing angle as a function of ρ is given by

$$\phi(\rho) = 17^\circ - \psi(\rho), \quad (5)$$

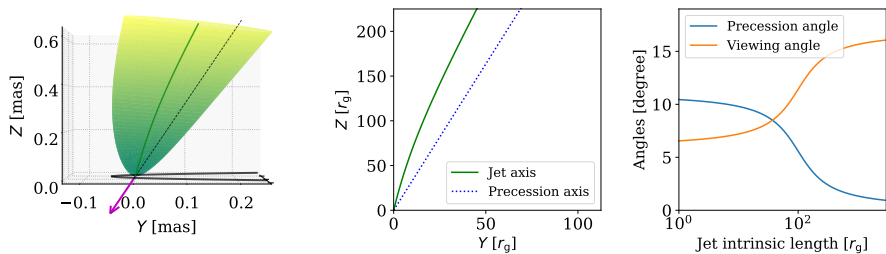


Fig. 5 *Left*: The 3D curved jet viewed edge-on, with symbols corresponding to those in the right panel of Fig. 3. The Y -axis represents the projected distance from the core, while the Z -axis means the distance from the core along LOS (positive means pointing towards us). *Middle*: The jet axis projected onto a 2D plane, providing a clearer view of its curvature. *Right*: Profiles of the precession angle and the viewing angle.

assuming $\psi < 17^\circ$. The value of 17° is adopted from the literature [17, 24, 37]. Similar to the standard case, we project the curved jet onto the X - Y to derive the observed jet width as a function of the measured axial distance.

The projected jet width is determined analytically. The equation for the surface of the curved jet is derived as follows. First, each point A on the original jet axis is mapped to a corresponding point A' on the curved axis, maintaining the same intrinsic length ρ . We denote the Y - and Z -coordinate of A' as ρ_y and ρ_z , respectively. The original jet cone is divided into rings of constant z (which corresponds the length along the jet axis). Each ring is first shifted to the origin by a vector $(0, 0, -\rho)$, rotated by an angle $\phi(\rho)$, and then shifted again by a vector $(0, \rho_y, \rho_z)$. The resulting ring satisfies the following equations

$$x^2 + \frac{(y - \rho_y)^2}{\cos^2 \phi} - C^2 \rho^{2\alpha} = 0, \quad (6)$$

$$z = \rho_z - \frac{\sin \phi}{\cos \phi} (y - \rho_y). \quad (7)$$

These transformed rings collectively form the surface of the curved jet. The observed jet width at a given measured jet axial distance y is twice the maximum X -coordinate on the curved jet's surface. From Eq. (6), the value of ρ that maximizes x for a given y satisfies the equation

$$(y - \rho_y) \frac{\sin \phi}{\cos^2 \phi} + \alpha C^2 \rho^{2\alpha-1} - (y - \rho_y)^2 \frac{\sin \phi}{\cos^3 \phi} \frac{d\phi}{d\rho} = 0. \quad (8)$$

The observed jet width can then be calculated as:

$$W(y) = 2 \times \left(C^2 \rho^{2\alpha} - \frac{(y - \rho_y)^2}{\cos^2 \phi} \right)^{1/2}. \quad (9)$$

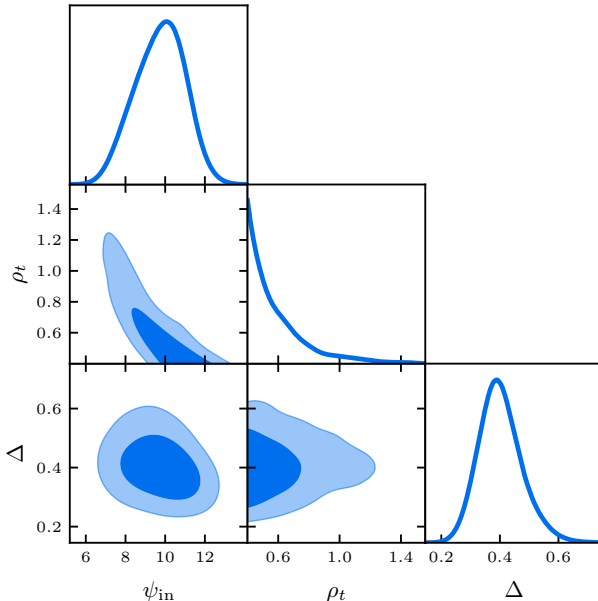


Fig. 6 Results of the MCMC analysis for the curved jet model, compared with the projected jet width profile measured by Lu et al. (2023) [23].

An example of $W(y)$ for both a curved jet and a tilted, collimated jet is shown in the left panel of Fig. 3, represented by the solid and dashed curves, respectively. The observed jet width is larger for a curved jet compared to a collimated one. This occurs because, with a smaller viewing angles, the same measured axial distance y corresponds to a longer intrinsic jet length ρ , resulting in a wider jet.

We performed a Markov Chain Monte Carlo (MCMC) analysis of the curved jet model, comparing it with the jet width profile measured by Lu et al. (2023) [23]. The results are presented in Fig. 6. Current jet width observations do not uniquely constrain the transition parameters, as there is a degeneracy between the transition position ρ_t and the innermost precession angle ψ_{in} . A smaller ρ_t , combined with a larger ψ_{in} , can yield the same observed jet width profile. To mitigate this degeneracy, we introduced a physical prior of $\rho_t > 100 r_g$ in the MCMC analysis, based on simulations that show the jet direction within $\lesssim 100 r_g$ remains perpendicular to the accretion disk [28].

To predict the evolution of the position angle, viewing angle, and jet width at a distance of 0.02 mas from the core, we first note that this scale is closer to the core than the transition region. Therefore, we approximate the jet at this scale using a fixed precession angle. Any minor discrepancies from this approximation are addressed by introducing an effective precession angle, which matches the measured jet width in 2018. At different times, the position and viewing angles are calculated following the method in Cui et al. (2023) [24],

while the jet width is determined based on the previously outlined method, taking into account the evolution of the viewing angle.

Note. Our results (and the interpretation in [24]) on the M87 SMBH spin and disk size are quite different from the recent work [38]. These differences are rooted in the way the jet precession is generated. While they assumed the dynamics of the jet only follows a ring at the warp radius that precesses independently, our interpretation is based on recent numerical simulations that found a bulk of the disk and the jet precesses coherently.

Acknowledgements. We thank Kazuhiro Hada and Mareki Honma for valuable discussion and comments and Rusen Lu for sharing the measurements of the jet width from Lu et al. 2023. W. L. acknowledges that this work is supported by the “Science & Technology Champion Project” (202005AB160002) and the “Top Team Project” (202305AT350002), both funded by the “Yunnan Revitalization” (202401AT070489). Y. C. is supported by the Natural Science Foundation of China (grant 12303021) and the China Postdoctoral Science Foundation (No. 2024T170845).

References

- [1] Curtis, H. D. Descriptions of 762 Nebulae and Clusters Photographed with the Crossley Reflector. *Publications of Lick Observatory* **13**, 9–42 (1918).
- [2] Igumenshchev, I. V., Narayan, R. & Abramowicz, M. A. Three-dimensional Magnetohydrodynamic Simulations of Radiatively Inefficient Accretion Flows. *Astrophys. J.* **592**, 1042–1059 (2003).
- [3] Yuan, F. & Narayan, R. Hot Accretion Flows Around Black Holes. *Annu. Rev. Astron. Astrophys.* **52**, 529–588 (2014).
- [4] Event Horizon Telescope Collaboration. First M87 Event Horizon Telescope Results. V. Physical Origin of the Asymmetric Ring. *Astrophys. J. Lett.* **875**, L5 (2019).
- [5] Event Horizon Telescope Collaboration. First M87 Event Horizon Telescope Results. VIII. Magnetic Field Structure near The Event Horizon. *Astrophys. J. Lett.* **910**, L13 (2021).
- [6] Reynolds, C. S. The spin of supermassive black holes. *Classical and Quantum Gravity* **30**, 244004 (2013).
- [7] Risaliti, G. *et al.* A rapidly spinning supermassive black hole at the centre of NGC 1365. *Nature* **494**, 449–451 (2013).
- [8] McClintock, J. E. *et al.* The Spin of the Near-Extreme Kerr Black Hole GRS 1915+105. *Astrophys. J.* **652**, 518–539 (2006).

- [9] McClintock, J. E., Narayan, R. & Steiner, J. F. Black Hole Spin via Continuum Fitting and the Role of Spin in Powering Transient Jets. *Space Sci. Rev.* **183**, 295–322 (2014).
- [10] Event Horizon Telescope Collaboration. First M87 Event Horizon Telescope Results. I. The Shadow of the Supermassive Black Hole. *Astrophys. J. Lett.* **875**, L1 (2019).
- [11] Blandford, R. D. & Znajek, R. L. Electromagnetic extraction of energy from Kerr black holes. *Mon. Not. R. Astron. Soc.* **179**, 433–456 (1977).
- [12] Blandford, R. D. & Payne, D. G. Hydromagnetic flows from accretion disks and the production of radio jets. *Mon. Not. R. Astron. Soc.* **199**, 883–903 (1982).
- [13] Junor, W., Biretta, J. A. & Livio, M. Formation of the radio jet in M87 at 100 Schwarzschild radii from the central black hole. *Nature* **401**, 891–892 (1999).
- [14] Dodson, R., Edwards, P. G. & Hirabayashi, H. Milliarcsecond-Scale Spectral Properties and Jet Motions in M 87. *Publ. Astron. Soc. Jpn* **58**, 243–251 (2006).
- [15] Hada, K. *et al.* An origin of the radio jet in M87 at the location of the central black hole. *Nature* **477**, 185–187 (2011).
- [16] Hada, K. *et al.* High-sensitivity 86 GHz (3.5 mm) VLBI Observations of M87: Deep Imaging of the Jet Base at a Resolution of 10 Schwarzschild Radii. *Astrophys. J.* **817**, 131 (2016).
- [17] Walker, R. C., Hardee, P. E., Davies, F. B., Ly, C. & Junor, W. The Structure and Dynamics of the Subparsec Jet in M87 Based on 50 VLBA Observations over 17 Years at 43 GHz. *Astrophys. J.* **855**, 128 (2018).
- [18] Kim, J. Y. *et al.* The limb-brightened jet of M87 down to the 7 Schwarzschild radii scale. *Astron. Astrophys.* **616**, A188 (2018).
- [19] Kravchenko, E. *et al.* Linear polarization in the nucleus of M87 at 7 mm and 1.3 cm. *Astron. Astrophys.* **637**, L6 (2020).
- [20] EHT MWL Science Working Group & Event Horizon Telescope Collaboration. Broadband Multi-wavelength Properties of M87 during the 2017 Event Horizon Telescope Campaign. *Astrophys. J. Lett.* **911**, L11 (2021).
- [21] Ro, H. *et al.* Transverse oscillations of the m87 jet revealed by kava observations. *Galaxies* **11** (2023).

- [22] Event Horizon Telescope Collaboration *et al.* The persistent shadow of the supermassive black hole of M 87. I. Observations, calibration, imaging, and analysis. *Astron. Astrophys.* **681**, A79 (2024).
- [23] Lu, R.-S. *et al.* A ring-like accretion structure in M87 connecting its black hole and jet. *Nature* **616**, 686–690 (2023).
- [24] Cui, Y. *et al.* Precessing jet nozzle connecting to a spinning black hole in M87. *Nature* **621**, 711–715 (2023).
- [25] Lense, J. & Thirring, H. Über den Einfluß der Eigenrotation der Zentralkörper auf die Bewegung der Planeten und Monde nach der Einsteinschen Gravitationstheorie. *Physikalische Zeitschrift* **19**, 156 (1918).
- [26] Fragile, P. C. & Anninos, P. Hydrodynamic Simulations of Tilted Thick-Disk Accretion onto a Kerr Black Hole. *Astrophys. J.* **623**, 347–361 (2005).
- [27] Fragile, P. C., Blaes, O. M., Anninos, P. & Salmonson, J. D. Global General Relativistic Magnetohydrodynamic Simulation of a Tilted Black Hole Accretion Disk. *Astrophys. J.* **668**, 417–429 (2007).
- [28] McKinney, J. C., Tchekhovskoy, A. & Blandford, R. D. Alignment of Magnetized Accretion Disks and Relativistic Jets with Spinning Black Holes. *Science* **339**, 49 (2013).
- [29] Liska, M., Tchekhovskoy, A., Ingram, A. & van der Klis, M. Bardeen-Petterson alignment, jets, and magnetic truncation in GRMHD simulations of tilted thin accretion discs. *Mon. Not. R. Astron. Soc.* **487**, 550–561 (2019).
- [30] Franchini, A., Lodato, G. & Facchini, S. Lense–Thirring precession around supermassive black holes during tidal disruption events. *Mon. Not. Roy. Astron. Soc.* **455**, 1946–1956 (2016).
- [31] Bardeen, J. M., Press, W. H. & Teukolsky, S. A. Rotating Black Holes: Locally Nonrotating Frames, Energy Extraction, and Scalar Synchrotron Radiation. *Astrophys. J.* **178**, 347–370 (1972).
- [32] Liu, S.-M. & Melia, F. Spin - induced disk precession in the supermassive black hole at the Galactic Center. *Astrophys. J. Lett.* **573**, L23 (2002).
- [33] Fragile, P. C. Effective Inner Radius of Tilted Black Hole Accretion Disks. *Astrophys. J. Lett.* **706**, L246–L250 (2009).
- [34] Asada, K. & Nakamura, M. The Structure of the M87 Jet: A Transition from Parabolic to Conical Streamlines. *Astrophys. J. Lett.* **745**, L28

(2012).

- [35] Nakamura, M. *et al.* Parabolic Jets from the Spinning Black Hole in M87. *Astrophys. J.* **868**, 146 (2018).
- [36] Pu, H.-Y., Yun, K., Younsi, Z. & Yoon, S.-J. Odyssey: A Public GPU-based Code for General Relativistic Radiative Transfer in Kerr Spacetime. *Astrophys. J.* **820**, 105 (2016).
- [37] Mertens, F., Lobanov, A. P., Walker, R. C. & Hardee, P. E. Kinematics of the jet in M 87 on scales of 100-1000 Schwarzschild radii. *Astron. Astrophys.* **595**, A54 (2016).
- [38] Wei, S.-W., Zou, Y.-C., Zhang, Y.-P. & Liu, Y.-X. Constraining black hole parameters with the precessing jet nozzle of M87*. *Phys. Rev. D* **110**, 064006 (2024).